Communication

Room temperature single-photon emission and lasing for all-inorganic colloidal perovskite quantum dots

Xiaosheng Tang [a], Zhiping Hu [a], Weiwei Chen [a], Xin Xing [b], Zhigang Zang [a,*], Wei Hu [a], Jing Qiu [a], Juan Du [b,**], Yuxin Leng [b,e], Xiaofang Jiang [c], Liqiang Mai [d]

[a] Key Laboratory of Optoelectronic Technology & Systems (Ministry of Education), Chongqing University, Chongqing 400044, China
[b] State Key Laboratory of High Field Laser Physics, Shanghai Institute of Optics and Fine Mechanics, Chinese Academy of Sciences, Shanghai 201800, China
[c] Institute of Polymer Optoelectronic Materials and Devices State Key Laboratory of Luminescent Materials and Devices, South China University of Technology, Guangzhou 510640, PR China
[d] Department of Materials Science & Engineering, Wuhan University of Technology, China
[e] School of Physical Science and Technology, Shanghai Tech University, Shanghai 201210, China

ARTICLE INFO

ABSTRACT

Recent reports regarding metal halide semiconductors of perovskite nanocrystal structures have presented us a promising future on their optoelectronic applications such as laser and light harvesting devices. In this paper, all-inorganic perovskites $CsPbX_3$ (X=Cl, Br and I) quantum dots (QDs) with tunable fluorescence from 400 nm to 700 nm were prepared by a facile hot-injection method. Besides, random lasing with coherent feedback was observed in films of $CsPbX_3$ QDs. Under 400 nm optical excitation at room temperature, sharp lasing peaks emission at around 427 nm, 527 nm and 539 nm with low pump thresholds intensity were achieved by halide substitution. The dynamic fluorescence from one single quantum dot also was detailed investigated. These results demonstrated that all-inorganic perovskites could be used as low-threshold and wavelength-tunable gain materials for lasing application at room-temperature.

1. Introduction

Over the last decade, quantum dots (QDs) have been intensively studied as future optoelectronic materials due to their many attractive properties [1], including size-tunable band gap [2], high photoluminescence (PL) quantum yields (QYs) [3], excellent photostability [4], and versatile chemical processability [5]. The most well-known example is CdSe quantum dots, whose fluorescence wavelength can be tuned throughout the whole visible spectrum by changing the size around two nanometers [5,6]. Furthermore, excellent and repetitive optical properties of CdSe/CdS core/shell QDs with PL QYs up to > 90% has been analyzed by Wennuan Nan and his coworkers [7]. Recently, a new class of QDs based on lead halide perovskites, generally known as a versatile material, has attracted significant attention for its intriguing properties such as shallow defect, high light absorption coefficient ($105\ cm^{-1}$) and long diffusion length. Moreover, it also has been proved to have promising applications upon device fabrication including solar cells [8–10], light emitting diodes (LEDs) [11–13],

and lasers [14–16]. As one class of the QDs, perovskite nanocrystals are tremendously drawn attention because of their excellent optoelectronic properties. In particular, hybrid organic-inorganic lead halide perovskites $CH_3NH_3PbX_3$ (X=Cl, Br, and I) thin film solar cells with more than efficiency of 20% have reported in recent years in recent years [17]. On the other side, the studies on electrically driven light-emitting diodes and optical gain media for lasing applications based on perovskites $CH_3NH_3PbX_3$ nanomaterials have drawn much attention [18,19].

Although there are promising developments of organic-inorganic lead halides perovskite nanocrystal materials because of their attractive properties, the problem of their unsolved photostability has greatly hampered their further practical and commercial applications [20]. As one kind of perovskite materials, all-inorganic $CsPbX_3$ have been regarded as one kind of potential substitutes for hybrid organic-inorganic perovskite $CH_3NH_3PbX_3$. Moreover, recent studies based on $CsPbX_3$ perovskite nanocrystals demonstrate that they have many notable advantages over organic-inorganic metal halide perovskite in terms of optoelectronic device [21,22]. For example, green LEDs have been fabricated using all-inorganic cesium lead halide perovskite nanocrystals as emitters, which led to the three-fold increase in peak brightness reaching $1377\ cd/m^2$, the highest reported value for $CsPbX_3$

colloidal nanocrystals (NCs) based LEDs so far [21]. The inorganic $CsPbI_3$ perovskite solar cells with current-voltage curve measured efficiency up to 2.9% and power conversion efficiency of 1.7% also have been fabricated, which is even more stable than the hybrid organic-inorganic materials [22]. This report highlights that the inorganic perovskite is unlikely to be essential for efficient perovskite solar cells [22]. Besides, several reports have indicated that all-inorganic $CsPbX_3$ (X=Cl, Br, and I) materials could probably be a potential candidates in the application of laser due to their high optoelectronic quality, especially for the $CsPbX_3$ (X=Cl, Br, and I) NCs [23–25]. There are a few reports about the all-inorganic perovskite nanomaterials including size control, shape adjustment, and optoelectronic device applications [21–27]. Despite all-inorganic perovskite $CsPbX_3$ have superior properties as well as organic-inorganic perovskite materials, whereas, most of the studies about all-inorganic perovskite nanocrystals mainly focused on the fabrications of these materials such as quantum dots and nanowires [28,29]. After literature review, it could be found that there are only few studies about lasing application based on all-inorganic $CsPbX_3$. There is also few experimental results about the dynamic fluorescence from one single quantum dot. Therefore, it is still a challenging task to prepare $CsPbX_3$ for low-threshold and wavelength-tunable laser application.

In this work, a hot-injection method to fabricate all-inorganic perovskite $CsPbX_3$ QDs with tunable photoluminescence (400–700 nm) was demonstrated. Moreover, the as-prepared $CsPbX_3$ nanoparticles exhibited good crystal quality and low-threshold amplified spontaneous emission. Sharp lasing peaks emission at around 427 nm, 527 nm and 539 nm with low pump thresholds intensity were achieved. The peak of lasing emission spectra in blue region can reach ~427 nm. Furthermore, the dynamic fluorescence from one single quantum dot shows good photostability of all-inorganic perovskite nanoparticles under ambient environment.

2. Experiments

2.1. Fabrication of CsPbX₃ QDs

To prepare the crude solution, a mixture of 100 mg Cs_2CO_3, 0.6 ml of oleic acid (OA), and 5 ml of octadecene (ODE) was degassed under nitrogen flow in a three-neck flask at 120 °C for 1 h until all the Cs_2CO_3 reacted with OA. 5 ml ODE and 0.36 mmol of PbX_2 (X=Cl, Br and I) or their mixtures were mixed in a 100 ml three-necked flask which was placed in a heating jacket with nitrogen. This three-necked flask was heated to 120 °C under nitrogen flow for 1 h. Then the temperature was set up to 150 °C. 0.5 ml oleylamine (OLA) and 0.5 ml OA were injected into the PbX_2 crude solution quickly when the temperature reached 150 °C. After complete solubilisation of PbX_2 salts, 0.4 ml Cs-precursor solution was swiftly injected. The reaction kept for ~10 s, and then was cooled by the ice bath. For the isolation and purification of $CsPbX_3$ NCs, the nanocrystals crude solution was centrifuged and precipitated by dissolving in toluene. After 3–4 centrifugations, the supernatant was discarded and the particles were dispersed in toluene forming long-term stable solutions.

2.2. Characterization of CsPbX₃

The crystal phases of all samples were characterized by X-ray diffraction (XRD) with CuKa radiation (XRD-6100, SHIMADZU, Japan). The transmission electron microscopy was recorded using a ZEISS LIBRA 200FE microscope. The absorption spectra were adopted by a Scan UV–vis spectrophotometer (UV–vis: UV-2100, Shimadzu, Japan). The spectra were recorded at room temperature ranging from 200 to 800 nm. The photoluminescence spectroscopy were measured by a fluorescence spectrophotometer (PL: Agilent Cary Eclipse, Australia) which included a Xe lamp as an excitation source with optical filters.

2.3. Lasing experiment

For the lasing measurements, a femtosecond amplified laser system was employed as the pumping source. The optical wavelength of 400 nm was generated by frequency-doubling of output pulse (Wavelength: 800 nm, Repetition rate: 1 kHz, Pulse-width: 100 fs) from regenerative amplifier using β-barium borate (BBO) crystal.

3. Results and discussion

The $CsPbX_3$ nanoparticles prepared here are fabricated following a recipe slightly modified from the literature [29], which take advantages of the ionic nature of the chemical bonding in these compounds. $CsPbX_3$ are known to crystallize in orthorhombic, tetragonal, and cubic polymorphs of the perovskite lattice with the cubic phase for all compounds [29–32]. In our work, the XRD data (Fig. 1a) show that the nanocrystals have a well-defined three-dimensional structure, which agreed well with the formation of $CsPbX_3$ QDs. As shown in the X-ray diffraction (XRD) of the $CsPbX_3$ QDs, all $CsPbX_3$ NCs crystallize in the cubic phase [30], which could be attributed to the combined effect of the high synthesis temperature and contributions from the surface energy. The typical cubic crystal structure diagram of $CsPbX_3$ represented by $CsPbBr_3$ is shown in Fig. S1 in Supporting information. To investigate the morphology and composition of the $CsPbX_3$ QDs, the transmission electron microscope (TEM) (Fig. 1b), high resolution transmission electron microscope (HRTEM) image (Fig. 1c) and the energy dispersion spectrometry (EDS) (Fig. 1d) of $CsPbBr_3$ QD are presented. Fig. 1b shows a TEM image of $CsPbBr_3$ QD as well as the size distribution. It is observed that typical $CsPbBr_3$ QDs have an average diameter of ~9.0 nm (inset figure). The HRTEM (Fig. 1c) image reveals that the interplanar distance is 0.58 nm, corresponding to (110) planes, which is consistent with the XRD results. TEM and HRTEM information about $CsPbCl_3$ and $CsPb(Cl/Br)_3$ are also shown in Fig. S2. In comparison with $CsPbBr_3$ QDs, the $CsPbCl_3$ and $CsPb(Cl/Br)_3$ nanoparticles demonstrated the similar shape, and the size distribution showed it is about 8 and 8.5 nm. From the HRTEM images of Fig. S2b and d, the interplanar distance of $CsPbCl_3$ and $CsPb(Cl/Br)_3$ was about 0.51 and 0.54 nm, which could be ascribed to the (110) planes [33–35]. The energy-dispersive spectroscopy (EDS) (Fig. 1d) measurement shows that $CsPbBr_3$ nanoparticles have a Br/Cs and Br/Pb molar ratio of ~1.0 and 3.9 respectively, which agrees well with the stoichiometry ratio.

Through compositional modulations, the band gap energies and photoluminescence are tunable over the entire visible spectral region from 400 nm to 700 nm(Fig. 2a). The optical images of colloidal solutions in toluene under ultraviolet lamp are from blue to red, when excited by 365 nm (Xe lamp) (Fig. S3), which are consistent with PL spectra. Remarkably bright PL of all QDs is characterized by narrow emission line widths of 12–25 nm. The optical absorption and emission spectra of $CsPbBr_3$ NC film are showed in Fig. 2b, which have small stokes shift. The PL peak wavelength of $CsPbBr_3$ NCs is centered at ~527 nm (Fig. 2b). Through the injection of Cl ions, the wavelength of emission shifts to ~400 nm. Instead, the PL wavelength has red shift after injecting I ions. As well as the PL spectra, the absorption spectra of $CsPbX_3$ also cover the entire visible spectral region (Fig. S4).

Fluorescence intermittency, also referred as blinking, randomly switching between states of high (ON) and low (OFF) emissions, is
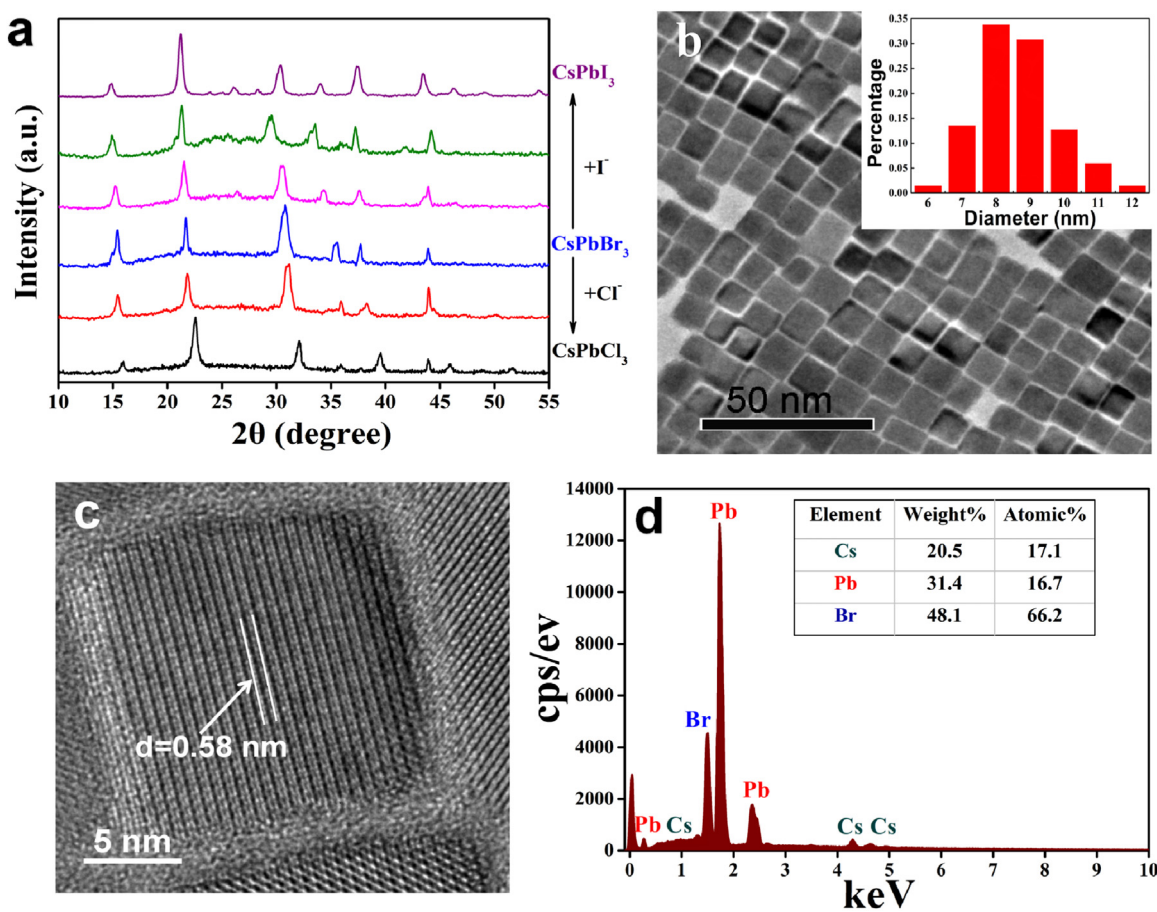
Fig. 1. (a) The XRD of the CsPbX$_3$ (X=Cl, Br and I) nanoparticles with different composition. (b) TEM image of the CsPbBr$_3$ nanoparticles, the scale bar is 50 nm, the inset figure is the size distribution of the CsPbBr$_3$ nanoparticles in b. (c) HRTEM image of CsPbBr$_3$ nanoparticles, and the scale bar is 5 nm. (d) The EDS of the CsPbBr$_3$ nanoparticles.
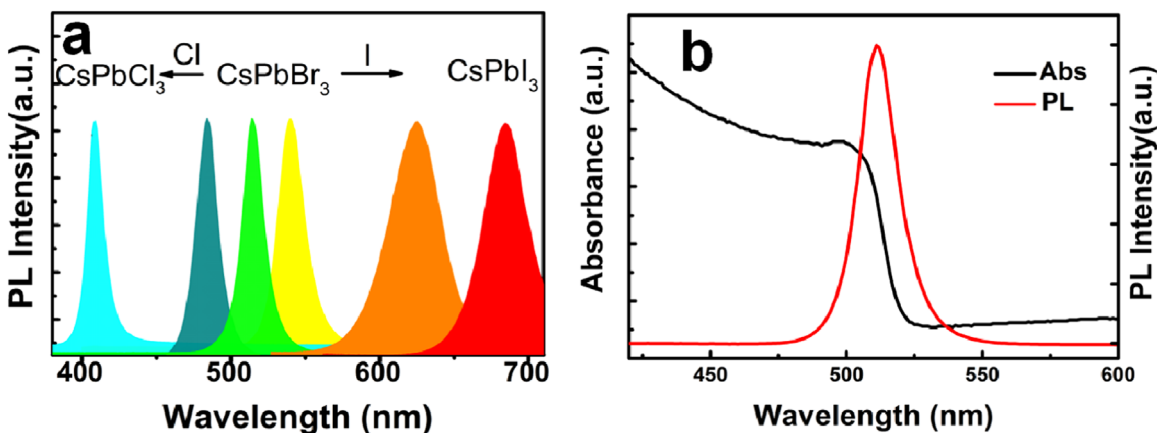

Fig. 2. (a) The PL spectra of the CsPbX$_3$ NC film with different compositions. (b) The absorption (black) and PL spectra (red) of CsPbBr$_3$ NC film.

a universal property of molecular emitters found in nanostructures, such as nanocrystals, carbon nanotubes, and nanorods [36,37]. It has been demonstrated that the CsPbX$_3$-based perovskite QDs can serve as room-temperature sources of single photons [38]. In order to better understand the dynamic fluorescence, the "blinking" property from one single quantum dot should be investigated in detail. To obtain complete information about the fluorescence dynamics of single CsPbX$_3$ QD, the sample of CsPbBr$_3$ QD is excited by 405 nm continuous wave laser. This method has been described in detail in our previous work [39]. For single-nanoparticle measurements, a dilute solution of QDs is mixed with

toluene and spin coated onto a glass substrate. Dark-field scattering microscopy is utilized to locate the particles of interest (Fig. 3a). Each bright spot corresponds to single CsPbBr$_3$ QD or a cluster of several CsPbBr$_3$ QDs. Here we focus laser onto a single bright spot by an oil-immersed objective (100×, NA=0.5), to obtain fluorescence intensity time trace (100 ms bin time) (Fig. 3b, spectrum 2). Fluorescence signal is also collected by the objective (100×, NA=0.5), and filtered by 442 nm long pass filter. To detect the fluorescence intensity fluctuation of QD, an avalanche photodiode (Perkin Elmer, SPCM-AQR-14) coupled with PicoHarp 300 is used. In this measurement, to exclude the emission from the
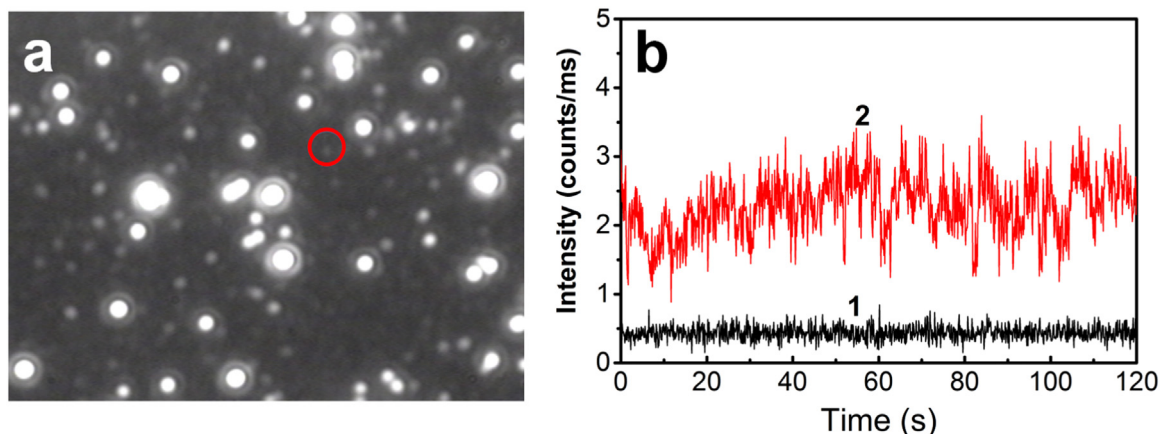
Fig. 3. (a) Dark-field scattering image of CsPbBr$_3$ NCs film with low particle concentration. (b) The dynamic fluorescence intensity time trace recorded for CsPbBr$_3$ QD (circle in a) of several CsPbBr$_3$ QDs with 100 ms per bin, using 405 nm continuous wave laser as excitation source.

background, we set a glass substrate without sample as comparison, which has no emission intensity (Fig. 3b, spectrum 1). As shown in spectrum 2, the overall intensity of ON state has no obvious decrease with time, indicating that no signatures of degradation are observed with exposure under laser light. In spectrum 2, the measured fluorescence intensity from QDs fluctuates between two levels: high emissivity (ON) and low-emissivity (OFF), as well as other colloidal QDs observed previously [40–42]. This observation about the emission from individual QDs exhibits strong photon antibunching under continuous-wave (cw). As in the case of other known colloidal QDs, the antibunching arises from fast Auger recombination [43,44]. In spectrum b, the average signal from ON state is higher than that of OFF state after the dot freshly exposed to laser light for the reason of the stable structure of CsPbBr$_3$ QDs with a small number of generations of surface defects under the exposure to laser light. Since the surface defects act as centers for nonradiative recombination, the reduction of the semiconductor core of QDs leads to an increase of the band gap energy. Nonradiative recombination is also observed by the time-resolved PL decay curves from CsPbBr$_3$ QDs under 400 nm pulsed excitation (Fig. S5). According to the time-resolved PL decays of CsPbCl$_3$, CsPb(Cl/Br)$_3$ and CsPbBr$_3$ QDs (Fig. S5), the τ_r, τ_{nr} (nonradiative lifetime) and τ (average lifetime) are calculated in Table S1, which indicate that τ_r (radiative lifetime) of CsPbBr$_3$ (PL peak at $\sim$527 nm) is longer than that of CsPbCl$_3$ QD (PL peak at $\sim$408 nm), which is consistent with the results reported before [34].

Many potential applications of semiconductor nanocrystals are hindered by nonradiative Auger recombination wherein the electron-hole recombination energy is transferred to a third charge carrier. This process severely limits the bandwidth of optical gain, leads to large nonradiative losses, which is believed to be responsible for blinking of emission from single nanocrystals. In the present work, despite the highly efficient intrinsic nonradiative Auger recombination of CsPbBr$_3$ QDs, random lasing can also be developed under atmospheric environment through modified pumping configuration. To explore the stimulated emission, CsPbBr$_3$ QD films are spin coated on glass at atmospheric environment. The thickness of the film is about 550–750 nm according to scanning electron microscope (SEM) image of the homogeneous and compact CsPbBr$_3$ NC film (Fig. S6). Then the close-packed thin film of CsPbBr$_3$ QDs is excited by 1 kHz, 100 fs laser pulses centered at 400 nm, as shown in Fig. 4c. The excitation is kept at low intensity to avoid the complication of re-absorption and amplification effects, and the measurements are performed at room temperature.

As is well known, the lasing action is a phenomenon that the

photoluminescence stimulated emission (SE) overcome the spontaneous emission at some excitation level. Below the lasing threshold, the photoluminescence power rises slowly as the excitation power increases. Above the lasing threshold, as a lasing evidence, the slope of power vs excitation becomes orders of magnitude greater. In addition, the bandwidth of the lasing emission is orders of magnitude narrower compared with the one below lasing threshold. From the reported results before, the linewidths of the laser from colloidal quantum dots were gradually developed, and most of the reported results were about several nanometers [45,46]. In this work, as shown in Fig. 4a, the pump-fluency dependence of the emission and the threshold behavior of CsPbBr$_3$ NC film, it is found that the PL spectra under low pump intensities ($<\sim$970 µJ/cm^2) is dominated by the relatively broad spontaneous emission located at $\sim$527 nm (full-width of half maximum (FWHM): $\sim$22 nm). When the pump intensity exceeds $\sim$970 µJ/cm^2, a narrower emission band located at $\sim$539 nm with FWHM of $\sim$6 nm appears on the longer wavelength side. This red-shifted stimulated emission may has its origins in re-absorbance during single-excition lasing [47,48] or in the exciton binding energies in the bi-exciton optical gain mechanism [49]. Fig. 4b shows the peak emission intensity as a function of the excitation intensity (left axis) and FWHM of the emission (right axis). Around the lasing threshold $\sim$0.97 mJ/cm^2, it could be observed that an obvious transition change in gradient of the PL intensity curve and a sharp decrease for FWHM. Fig. 4d shows the real color optical images of CsPbBr$_3$ NC film photoexcited with above lasing threshold fluorescence. We can observe the random lasing from the sample.

It is known that the band gap of lead halide perovskites could be tuned by changing their constituent stoichiometry. Fig. 4e–g display the blue and green stimulated emission from CsPbBr$_x$/Cl$_{3-x}$ QDs (x=0, 2, 3), respectively. The spectra of CsPbCl$_3$ (Fig. 4e) and CsPbBr$_2$/Cl$_1$ (Fig. 4f) films also have red shift as well as CsPbBr$_3$ film (Fig. 4g). In Fig. 4e, the wavelength of lasing for CsPbCl$_3$ is at $\sim$427 nm with $\sim$6 nm FWHM when the pump intensity is high ($>\sim$1.90 mJ/cm^2). The peak of spectra in blue region could reach $\sim$408 nm. When the pump intensity is above the threshold, the lasing emission peak achieved $\sim$427 nm with 11 nm shift (Fig. S7). The emission peak in blue region has blue shift to the report results [23]. As one systematic study based on the lasing application, the blue laser emission is an important part.

Although the lasing from quantum dots has been analyzed widely [50–52]. Unfortunately, the study about this exact mechanism for optical gain has been remaining question. This is also an open question in the MAPbX$_3$-related materials [51]. As is well known, effective optical feedback from a high-quality optical
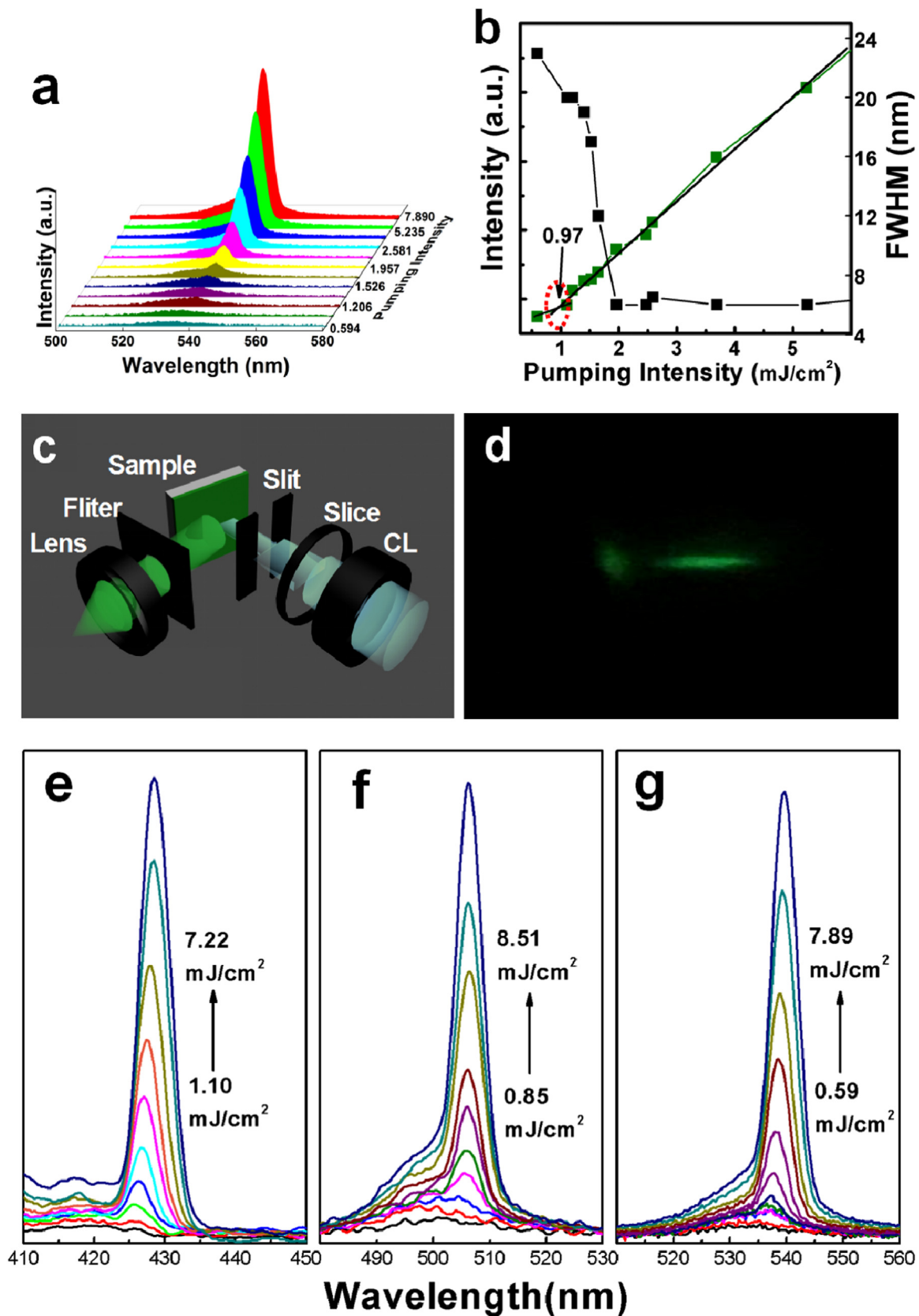
Fig. 4. (a) Pump-fluence dependence of the emission from CsPbBr$_3$ NCs film (pumping intensity range is 0.59–7.89 mJ/cm^2). (b) The lasing threshold behavior of the CsPbBr$_3$ NC film. (c) Schematic of the modified optical systems for pumping configuration, cylindrical lens (CL). (d) Photograph of CsPbBr$_3$ NC film excited above lasing threshold. (e–g) Pump-fluence dependence of the emission from CsPbX$_3$ (X=Cl, Br) NCs films. (e) CsPbCl$_3$ (pumping intensity range is 1.10–7.22 mJ/cm^2). (f) CsPb(Cl/Br)$_3$ (pumping intensity range is 0.85–8.51 mJ/cm^2). (g) CsPbBr$_3$ (pumping intensity range is 0.59–7.89 mJ/cm^2).
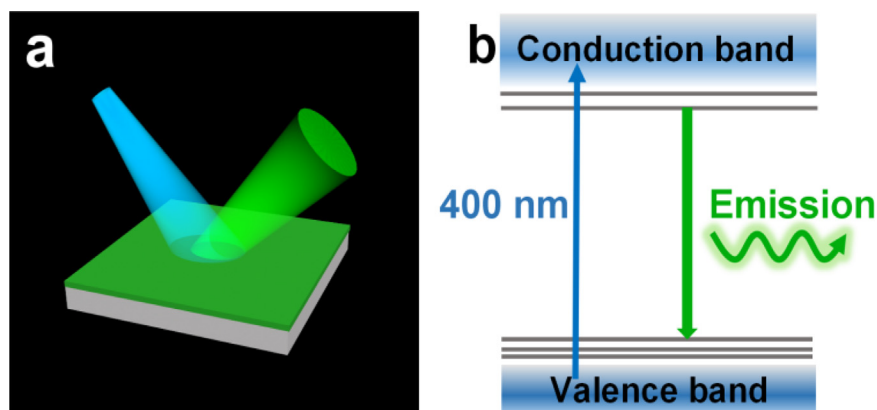
Fig. 5. (a) The schematic representation of CsPbX$_3$ NCs film excited by a focused 400 nm pulse laser. (b) Schematic diagram of the mechanism of optical gain with excitation.

resonator is needed to obtain lasing [18]. But lasing can also be obtained without optical resonators. When the required optical feedback is provided via light scattering induced by intrinsic disorder in the lasing medium, leading to so-called random lasing [51]. As shown in Fig. 5a, when CsPbX$_3$ NCs film is excited by a 400 nm pulse laser, random lasing could be obtained via light scattering caused by intrinsic disorder of CsPbX$_3$ QDs in the film. The mechanism of random lasing emission in CsPbX$_3$ NCs film could be explained as follows (Fig. 5b). We propose that light scattering phenomenon is significant in thicker films of several microns. When the CsPbX$_3$ NCs film is excited by pump light source, generated photons disperse in highly scattering media of CsPbX$_3$ QDs and randomly form closed loops. The generated photons propagate along the closed loops via coherent feedback, resulting in random fluctuations of lasing modes once the pump intensity over the threshold intensity. Furthermore, the high-quality (Q) factors of microlasers from CsPbX$_3$ NCs have been calculated in Table S2 in Supporting information. The Q factor around 539 nm is about 90. The low threshold and high Q factor probably could be attributed to a combined contribution of several factors, such as the large absorption cross-section, the high photoluminescence quantum yield, the ultrafast buildup of population inversion and subsequent optical amplification, and the large Stokes shift of the SE peak [23]. This not only provides the obvious technological advantage of facile and inexpensive fabrication, but also enables various applications such as displays and lighting, which derive from the their broad spectral angular distribution of the emission.

4. Conclusion

In summary, all-inorganic perovskite CsPbX$_3$ QDs are prepared by a facile hot-injection method. The dynamic PL from a single CsPbX$_3$ nanocrystal reveals that the as-prepared CsPbX$_3$ QDs are robust in atmospheric environment. The PL and amplified stimulated emission from CsPbX$_3$ films possess superior optical gain properties, representing a new class of low-threshold and wavelength-tunable gain materials without cavity. The peak of lasing emission spectra in blue region can reach ∼427 nm. All of these results suggest that all-inorganic perovskite CsPbX$_3$ QDs with good crystal quality are superior to traditional nanocrystals for lasing and optical amplification, benefiting from the broad spectral distribution and low pump threshold of the random lasing.

Appendix A. Supporting information

Supplementary data associated with this article can be found in the online version at http://dx.doi.org/10.1016/j.nanoen.2016.08.062.

References

[1] A.P. Alivisatos, K.P. Johnsson, X. Peng, T.E. Wilson, C.J. Loweth, M.P. Bruchez, P. G. Schultz, Science 271 (1996) 933–937.
[2] L.E. Brus, J. Chem. Phys. 80 (1984) 4403–4409.
[3] O. Chen, J. Zhao, V.P. Chauhan, J. Cui, C. Wong, D.K. Harris, H. Wei, H.S. Han, D. Fukumura, R.K. Jain, M.G. Bawendi, Nat. Mater. 12 (2013) 445–451.
[4] M. Nirmal, L. Brus, Acc. Chem. Res. 32 (1999) 407–414.
[5] D.V. Talapin, J.S. Lee, M.V. Kovalenko, E.V. Shevchenko, Chem. Rev. 110 (2010) 389–458.
[6] H.J. Yun, T. Paik, M.E. Edley, J.B. Baxter, C.B. Murray, ACS Appl. Mater. Interfaces 6 (2014) 3721–3728.
[7] W. Nan, Y. Niu, H. Qin, F. Cui, Y. Yang, R. Lai, X. Peng, J. Am. Chem. Soc. 134 (2012) 19685–19693.
[8] M.A. Green, A. Ho-Baillie, H.J. Snaith, Nat. Photonics 8 (2014) 506–514.
[9] H. Zhou, Q. Chen, G. Li, S. Luo, T. Song, H.S. Duan, Z. Hong, J. You, Y. Liu, Y. Yang, Science 345 (2014) 542–546.
[10] A. Kojima, K. Teshima, Y. Shirai, T. Miyasaka, J. Am. Chem. Soc. 131 (2009) 6050–6051.
[11] G. Li, Z.-K. Tan, D. Di, M.L. Lai, L. Jiang, J.H.W. Lim, R.H. Friend, N.C. Greenham, Nano Lett. 15 (2015) 2640–2644.
[12] Y.H. Kim, H. Cho, J.H. Heo, T.S. Kim, N. Myoung, C.L. Lee, S.H. Im, T.W. Lee, Adv. Mater. 27 (2015) 1248–1254.
[13] Z.K. Tan, R.S. Moghaddam, M.L. Lai, P. Docampo, R. Higler, F. Deschler, M. Price, A. Sadhanala, L.M. Pazos, D. Credgington, Nat. Nanotechnol. 9 (2014) 687–692.
[14] H. Zhu, Y. Fu, F. Meng, X. Wu, Z. Gong, Q. Ding, M.V. Gustafsson, M.T. Trinh, S. Jin, X.Y. Zhu, Nat. Mater. 14 (2015) 636–643.
[15] Q. Zhang, S.T. Ha, X. Liu, T.C. Sum, Q. Xiong, Nano Lett. 14 (2014) 5995–6001.
[16] G. Xing, N. Mathews, S.S. Lim, N. Yantara, X. Liu, D. Sabba, M. Grätzel, S. Mhaisalkar, T.C. Sum, Nat. Mater. 13 (2014) 476–480.
[17] W.S. Yang, J.H. Noh, N.J. Jeon, Y.C. Kim, S. Ryu, J. Seo, S.I. Seok, Science 348 (2015) 1234–1237.
[18] B.R. Sutherland, S. Hoogland, M.M. Adachi, C.T. Wong, E.H. Sargent, ACS nano 8 (2014) 10947–10952.
[19] X. Qin, H. Dong, W. Hu, Sci. China Mater. 58 (2015) 186–191.
[20] G.E. Eperon, S.N. Habisreutinger, B.J. Bruijnaers, J.J. van Franeker, D. W. deQuilettes, R.A. Janssen, ACS Nano 9 (2015) 9380–9393.
[21] X. Zhang, H. Lin, H. Huang, C.J. Reckmeier, Y. Zhang, W.C. Choy, A.L. Rogach, Nano Lett. (2016).
[22] G.E. Eperon, G.M. Paternò, R.J. Sutton, A. Zampetti, A.A. Haghighirad, F. Cacialli,

H.J. Snaith, J. Mater. Chem. A 3 (2015) 19688–19695.

[23] S. Yakunin, L. Protesescu, F. Krieg, M.I. Bodnarchuk, G. Nedelcu, M. Humer, G. D. Luca, M. Fiebig, W. Heiss, M.V. Kovalenko1, Nat. Commun. (2015), http://dx. doi.org/10.1038/ncomms9056.

[24] J. Pan, S.P. Sarmah, B. Murali, I. Dursun, W. Peng, M.R. Parida, J.K. Liu, L. Sinatra, N. Alyami, C. Zhao, E. Alarousu, T.K. Ng, B.S. Ooi, O.M. Bakr, O.F. Mohammed, J. Phys. Chem. Lett. 6 (2015) 5027–5033.

[25] L. Protesescu, S. Yakunin, M.I. Bodnarchuk, F. Krieg, R. Caputo, C.H. Hendon, M. V. Kovalenko, Nano Lett. 15 (2015) 3692–3696.

[26] S. Ji, X. Lei, L. Jian, X. Jie, D. Yu, L. Xiao, Z. Hai, Adv. Mater. (2016), 10.1002/ adma.201600225.

[27] L. Xiao, W. Ye, Z. Sheng, C. Bo, G. Yu, S. Ji, Z. Hai, Adv. Funct. Mater. (2016), http://dx.doi.org/10.1002/adfm.201600109.

[28] G. Nedelcu, L. Protesescu, S. Yakunin, M.I. Bodnarchuk, M.J. Grotevent, M. V. Kovalenko, Nano Lett. 15 (2015) 5635–5640.

[29] D. Zhang, S.W. Eaton, Y. Yu, L. Dou, P. Yang, J. Am. Chem. Soc. 137 (2015) 9230–9233.

[30] S. Sharma, N. Weiden, A.Z. Weiss, Phys. Chem. 75 (1992) 63–80.

[31] D.M. Trots, S.V. Myagkota, J. Phys. Chem. Solids 69 (2008) 2520–2526.

[32] C.C. Stoumpos, C.D. Malliakas, M.G. Kanatzidis, Inorg. Chem. 52 (2013) 9019–9038.

[33] P. Ramasamy, D.H. Lim, B. Kim, S.H. Lee, M.S. Lee, J.S. Lee, Chem. Commun. 52 (2016) 2067–2070.

[34] L. Protesescu, S. Yakunin, M.I. Bodnarchuk, F. Krieg, R. Caputo, C.H. Hendon, M. V. Kovalenko, Nano Lett. 15 (2015) 3692–3696.

[35] G. Nedelcu, L. Protesescu, S. Yakunin, M.I. Bodnarchuk, M.J. Grotevent, M. V. Kovalenko, Nano Lett. 15 (2015) 5635–5640.

[36] D. Canneson, L. Biadala, S. Buil, X. Quélin, C. Javaux, B. Dubertret, J.P. Hermier, Phys. Rev. B 89 (2014) 035303.

[37] T. Ihara, R. Sato, T. Teranishi, Y. Kanemitsu, Phys. Rev. B 90 (2014) 035309.

[38] Y.S. Park, S. Guo, N.S. Makarov, V.I. Klimov, ACS nano 9 (2015) 10386–10393.

[39] N. Gao, Y. Chen, L. Li, Z. Guan, T. Zhao, N. Zhou, Y. Pei, Q.Y. Shao, H. Xu, J. Phys. Chem. C 118 (2014) 13904–13911.

[40] A.V. Malko, Y.S. Park, S. Sampat, C. Galland, J. Vela, Y. Chen, J.A. Hollingsworth, V.I. Klimov, H. Htoon, Nano Lett. 11 (2011) 5213–5218.

[41] M. Nirmal, B.O. Dabbousi, M.G. Bawendi, J.J. Macklin, J.K. Trautman, T.D. Harris, L.E. Brus, Nature 383 (1996) 802–804.

[42] G. Xing, N. Mathews, S.S. Lim, N. Yantara, X. Liu, D. Sabba, T.C. Sum, Nat. Mater. 13 (2014) 476–480.

[43] A.M. Dennis, B.D. Mangum, A. Piryatinski, Y.S. Park, D.C. Hannah, J.L. Casson, J. A. Hollingsworth, Nano Lett. 12 (2012) 5545–5551.

[44] C. Javaux, B. Mahler, B. Dubertret, A. Shabaev, A.V. Rodina, A.L. Efros, D. R. Yakovlev, F. Liu, M. Bayer, G. Camps, Nat. Nanotechnol. 8 (2013) 206–212.

[45] C. Dang, J. Lee, C. Breen, J.S. Steckel, S. Coe-Sullivan, A. Nurmikko, Nat. Nano-technol. 7 (2012) 335–339.

[46] T.S. Kao, Y.H. Chou, C.H. Chou, F.C. Chen, T.C. Lu, Appl. Phys. Lett. 105 (2014) 1–5.

[47] C. Dang, A. Nurmikko, MRS Bull. 38 (2013) 737–742.

[48] J.Q. Grim, S. Christodoulou, F. Di Stasio, R. Krahne, R. Cingolani, L. Manna, I. Moreels, Nat. Nanotechnol. 9 (2014) 891–895.

[49] V.I. Klimov, A.A. Mikhailovsky, S. Xu, A. Malko, J.A. Hollingsworth, C. A. Leatherdale, M.G. Bawendi, Science 290 (2000) 314–317.

[50] D.S. Wiersma, Nat. Phys. 4 (2008) 359–367.

[51] R. Dhanker, A.N. Brigeman, A.V. Larsen, R.J. Stewart, J.B. Asbury, N.C. Giebink, Appl. Phys. Lett. 105 (2014) 1–5.

[52] Y. Wang, X. Li, J. Song, L. Xiao, H. Zeng, H. Sun, Adv. Mater. 27 (2015) 7101–7108.